Localized electropolymerization on oxidized boron-doped diamond electrodes modified with pyrrolyl units†

Paolo Actis,[ab] Mael Manesse,[a] Carolina Nunes-Kirchner,[c] Gunther Wittstock,[c] Yannick Coffinier,[de] Rabah Boukherroub[de] and Sabine Szunerits*[a]

Received 15th August 2006, Accepted 19th September 2006
First published as an Advance Article on the web 3rd October 2006
DOI: 10.1039/b611735j

This paper describes the functionalization of oxidized boron-doped diamond (BDD) electrodes with *N*-(3-trimethoxysilylpropyl)pyrrole (TMPP) and the influence of this layer on the electrochemical transfer kinetics as well as on the possibility of forming strongly adhesive polypyrrole films on the BDD interface through electropolymerization. Furthermore, localized polymer formation was achieved on the TMPP-modified BDD interface using the direct mode of a scanning electrochemical microscope (SECM) as well as an electrochemical scanning near-field optical microscope (E-SNOM). Depending on the method used polypyrrole dots with diameters in the range of 1–250 μm are electrogenerated.

1. Introduction

Boron-doped diamond (BDD) thin films show excellent mechanical properties, extreme chemical stability, good biocompatibility, good electrical conductivity, low background current densities and a large potential window in aqueous electrolytes (about −1.35 V to 2.3 V/NHE).[1,2] Consequently, they have found applications in electroanalysis,[3] in purification of wastewater,[4] and in biotechnology.[5–9] The electrochemical behavior of BDD electrodes is mainly influenced by two factors: the dopant concentration and the surface termination.[10–14] While doping levels between 10^{19}–10^{20} boron atoms cm^{-3} are mostly encountered for electrochemical applications, the surface termination of BDD electrodes can be diverse. As-deposited BDD surfaces are hydrogen-terminated with a hydrophobic character; they are stable in air without any apparent degradation for several months. These H-terminated BDD can be oxidized using various conditions[9,10,15–19] resulting in diamond electrodes composed of oxygen-containing functional groups such as ether (C–O–C), carbonyl (C═O) and surface hydroxyl (C–OH) groups. The surface hydroxyl groups (–OH) are of particular interest. While silane reagents show no reactivity towards carbonyl or ether groups, OH groups react specifically with different silane derivatives[10,17] to introduce chemical functionalities on the surface. The presence of surface hydroxyl groups on photochemically oxidized diamond surfaces was recently confirmed by the reaction with perfluorodecyl trichlorosilane [CF_3–$(CF_2)_7$–CH_2–CH_2–$SiCl_3$] for 2 h at room temperature under controlled atmosphere in hexane/CCl_4 (v/v 70/30, 10^{-2} M) solution.[10] Indeed, the functionalization of diamond surfaces by organic silane monolayers constitutes an attractive approach for designing well defined interfaces for numerous applications ranging from molecular electronics to chemical/biological sensing as already demonstrated on silicon surfaces.[20] The electrochemical behavior of silanized BDD surfaces is mostly characteristic of a highly efficient barrier for a redox probe.[21] Notsu *et al.*[17] showed however that the modification of BDD surface hydroxyl groups with 3-aminopropyltriethoxysilane (APTES) accelerates the $Fe(CN)_6^{4-/3-}$ redox reaction, compared to the oxygenated diamond. The observed effect was attributed to the electrostatic attraction between $Fe(CN)_6^{4-/3-}$ and protonated amino groups.

In this paper, we report on the functionalization of oxidized BDD surfaces with *N*-(3-trimethoxysilylpropyl)pyrrole (TMPP). The influence of this layer on the electrochemical transfer kinetics is discussed. The covalent linking of pyrrole units on the BDD surface enables the formation of a strongly adhesive polymer film through electropolymerization. Furthermore, formation of polypyrrole dots on the micrometer scale on the BDD surface through local polymerization was conducted using two different scan probe techniques: scanning electrochemical microscopy (SECM) and an electrochemically based scanning near-field optical microscopy (E-SNOM).

2. Experimental

2.1. Materials

Potassium ferrocyanide(II) trihydrate [$(K_4Fe(CN)_6 \cdot 3H_2O$], potassium chloride (KCl), hexane, chloroform, tetrachlorocarbon, ethanol, acetonitrile and acetone were purchased from Acros. *N*-(3-trimethoxysilylpropyl)pyrrole was obtained from

[a] *Laboratoire d'Electrochimie et de Physicochimie des Matériaux et des Interfaces (LEPMI), CNRS-INPG-UJF, 1130 rue de la piscine, BP 75, 38402 St. Martin d'Hères Cedex, France. E-mail: sabine.szunerits@lepmi.inpg.fr*
[b] *Laboratoire de Spectrométrie Physique, UMR5588, 140 Avenue de la physique, BP 87, 38402 Saint Martin d'Hères, France*
[c] *Carl Von Ossietzky University of Oldenburg, Departement of Chemistry and Institut of Chemistry and Biology of the Marine Environment, D-26111 Oldenburg, Germany*
[d] *Institut de Recherche Interdisciplinaire (IRI) FRE, CNRS-2963*
[e] *Institut d'Electronique, de Microélectronique et de Nanotechnologie (IEMN), CNRS-8520, Cité Scientifique, Avenue Poincaré, BP 60069, 59652 Villeneuve d'Ascq, France*
† The HTML version of this article has been enhanced with colour images.

Gelest Inc. (France). Pyrrole was purchased from Acros and 1 M stock solutions were prepared in HPLC grade acetonitrile and were kept at −20 °C.

2.2. Diamond samples

Two different types of diamond samples were used. Polycrystalline diamond layers were synthesized in our laboratory on a silicon high purity p-type wafer by microwave plasma-enhanced chemical vapor deposition (PECVD) in a conventional reactor.[22] The growth conditions used were as follows: substrate temperature 700–900 °C; total gas flow of a mixture of 0.7% methane in 100 cm^2 of hydrogen; total pressure in the reactor 20 Torr; microwave power 700 W. The dopant source was boron oxide set in a Pt crucible placed on the substrate holder near the silicon substrate. Before commencing the diamond growth, the silicon substrates were ultrasonically damaged with diamond powder in ethanol in order to improve the nucleation density. After deposition, the methane flow was stopped and the films were kept under hydrogen plasma for an additional 30 min. For 24 h of deposition, the film thickness reached 8 μm. The dopant concentration in the diamond layers, as estimated from Raman spectroscopy measurements is in the range 10^{19}–10^{20} B cm^{-3}. The film resistivity was $\leq$0.1 Ω cm as measured with a four-point probe. The as-deposited samples were further treated for half an hour with a hydrogen plasma under the following conditions: 100 cm^2 of hydrogen flux, 25 Torr reactor pressure with a 600 W microwave power leading to a sample surface temperature of about 700 °C. At the end of the plasma treatment, the microwave power was switched off and the samples were allowed to cool down under the hydrogen flux. Oxidized diamond samples were obtained through UV irradiation in air for 2 h using a low pressure mercury arc lamp as reported previously.[10]

Polycrystalline boron-doped polished, freestanding diamond films were purchased from Windsor Scientific (Slough, UK). Briefly, highly boron-doped polycrystalline CVD diamond layers were grown to a thickness higher than 500 μm by adding diborane to the methane and hydrogen source gases supplied to a microwave CVD reactor. The samples were polished both on the nucleation and the growth side to a mirror finish. The electrodes were supplied as 5 × 5 mm^2 square plates. The resulting samples have a bulk electrical resistance of about 0.75 mΩ. The average boron doping level of the material was reported to be about 5×10^{20} boron atoms cm^{-3} as determined by secondary ion mass spectroscopy (SIMS). Prior to use, samples were cleaned in 3 : 1 (v/v) concentrated H_2SO_4/H_2O_2 (30%) for 15 min, followed by copious rinsing with Milli-Q water, and then slightly polished using diamond past (0.3 μm) to obtain a smooth particle-free surface.

(*Caution: piranha solution reacts violently with organic materials; it must be handled with extreme care, followed by copious rinsing with deionized water*).

2.3. Silanization of oxygen-terminated BDD

Silanization of the oxidized diamond surfaces was carried out in a solution of *N*-(3-trimethoxysilylpropyl)pyrrole (10^{-3} M) in hexane/CCl_4 (70/30: v/v) for 3 d at room temperature.

2.4. Preparation of the electro-optical tip

Pulling of fibers. Optical fiber tips were prepared by stripping about 2 cm of the polymer coating from the end of the optical fiber (Fiber Optics, core diameter: 4 μm, cladding: 126 μm), rinsing the exposed portion of the fiber with absolute ethanol, and drying it. A pulsed CO_2 laser puller (P-2000, Sutter Instruments; 20 W maximum) was used and the pulling parameters were typically: heat: 256, velocity: 18, delay: 126, pull: 60, filament: 0.

Gold deposition. Gold was deposited with a speed of 60 rpm by vacuum evaporation onto the tapered end of the pulled fiber to a length of about 2 cm, while the fiber was rotated at an angle of 15° relative to the horizontal where the gold source was located. The thickness of the deposit was controlled by measuring the variation of the acoustic impedance of a piezoelectric quartz and was estimated as 50 nm.

Electrical insulation and exposure of the tip ends. For electrical contact of the gold-coated optical fiber, the deposited gold layer was connected to a gold wire (60 μm diameter, Goodfellow) with silver paint (SPI supplies) and left to dry for 5 min. The gold-coated optical fiber was coated with a cathodic electrophoretic paint (FT23-0303, BASF, Münster, Germany). The paint was diluted to 1 : 1 in volume with an aqueous solution of acetic acid (3 mM). Gold coated pulled optical fibers were dipped into the paint solution and deposited by scanning the potential from 0 to −2.5 V at a scan rate of 20 mV s^{-1} between the tip and a Cu coil (500 μm diameter, Goodfellow). Heat curing of the formed insulating film was achieved by heating at 200 °C for 20 min. The insulating layer shrinks during heating so that the sharp end of the tip is exposed while the wall of the tip is completely insulated. During curing, the fiber was held upwards. Second insulation was carried out using the same parameters, followed by the same curing to ensure any pinholes formed on the first curing were sealed. Between each curing step the tip was characterized using cyclic voltammetry (10 mM $Fe(CN)_6^{4-}$ in 0.1 M KCl, v = 10 mV s^{-1}). Tips with radii between 5 and 200 nm in diameter were aimed at. As the curing step has only a success rate of about 50%, a third layer was in some cases necessary.

2.4. Instrumentation

2.4.1. X-Ray photoelectron spectroscopy. X-Ray photoelectron spectroscopy (XPS) measurements were performed with an ESCALAB 220 XL spectrometer from vacuum Generators. A monochromatic Al Kα X-ray source (1486.6 eV) was operated in the CAE (constant analyser energy) mode (CAE = 100 eV for survey spectra and CAE = 40 eV for high resolution spectra), using the electromagnetic lens mode. The angle between the incident X-rays and the analyzer is 58°. The detection angle of the photoelectrons is 90°, as referenced to the sample surface.

2.4.2. Scanning electron microscopy. Electron microscopy was carried out with a LEO 982 field-emission scanning electron microscope (SEM) with an image resolution of 2.1 nm at 1 kV and 1.5 nm at 15 kV at the analytical working distance.

2.4.3. Electrochemical measurements. Cyclic voltammetric measurements were performed with a HEKA PG 340 ring-disk potentiostat (Lambrecht, Germany). The diamond film working electrode ($A \approx 0.315$ cm^2) was sealed against the bottom of a single compartment electrochemical cell by means of a rubber O-ring. Electric contact was made to a copper plate, through the bottom of the silicon substance where the diamond was deposited. Platinum and Ag/AgCl electrodes were used as counter and reference electrodes, respectively. An aqueous solution of $K_4Fe(CN)_6$ (10 mM) in KCl (0.1 M) was used for the electrochemical studies. The electrochemical responses were fitted to theoretical working curves using DigiSim 3.03.

For E-SNOM experiments an Autolab 30 (EcoChemie, Netherlands) potentiostat was used. The cell was constructed by gluing (epoxy glue, Fast Araldite, Bostik) an O-ring (15 mm diameter, 2 mm height) onto the BDD sample, which could contain a maximum volume of 500 μL. Reference and counter electrodes were fixed on the lower side of a metal ring which was placed on top of the O-ring. The metal ring was placed on top of the O-ring in such a way that the electrodes were as close as possible to the BDD surface. Here the counter electrode of the electrochemical cell is the electro-optical probe.

2.4.4. Scanning electrochemical microscope (SECM). A home-built SECM instrument was used to record the images. The SECM setup consists of a stepper motor positioning system (Märzhäuser), an ADC board (Plug-in Electronic) and bipotentiostat (CHI 700B). The motor position and data acquisition are controlled by a home-made program written in C++ language. All SECM experiments were carried out with a 25 μm diameter Pt UME fabricated according to ref. 23 All electrochemical studies used an Ag/AgCl/3 M KCl reference electrode (CH Instruments) and a Pt-wire counter electrode. All potentials reported here refer to the Ag/AgCl/3 M KCl reference electrode. The in-house software MIRA was used to process and analyze the data.

2.4.5. Electrochemical-scanning near field microscope (E-SNOM). The electro-optical probe was brought into the near field with the help of a home-build scanning near field microscope (SNOM) incorporating a tuning fork transducer (Fig. 6A) to which the electro-optical tip was glued in a manner similar to the feedback procedure developed by Karrai and Grober.[24] Briefly, the tip was mounted on one prong of a quartz crystal tuning fork (Farnell Components, 32.768 kHz, length of prong: 5 mm) and glued with epoxy glue (Fast Araldite, Bostik) while the tip protruded about 3 mm beyond the end of the tuning fork. Only this part of the tip was immersed into the solution while the tuning fork remained in air during the experiment. The fork was rigidly attached to a piezo-electronic vibrator (called the driving piezo), which vibrates at a frequency of 33 kHz with an amplitude of nearly 0.01 nm. The driving piezo vibrates the tuning fork and the electro-optical tip together, with the latter positioned perpendicular to the sample plane. The resonance frequency was measured by a DSP lock-in amplifier (EG&G Instruments). The rough positioning of the probe to the substrate was accomplished using inchworm motors, for fine resolution in the z directions, a 10 μm Z range and 130 μm XY range (Piezosystem Jena) piezoelectric pusher was used. The tip is approached in steps to the surface until the monitored tuning fork amplitude damped to a set point (taken as 90% of the original amplitude). At this point the tip is some nm away from the surface. The tip–sample distance was controlled by controlling the tuning fork amplitude.

2.4.6. Determination of the far field radiation angular distribution. The far field radiation angular distribution transmitted by the optical tip is measured using a home-build goniometer, similar to that developed by Obermuller *et al.*[25]

2.4.7. Confocal imaging of the polymer dots. Quality control of the polymerization process was carried out using a confocal laser-scanning microscope (CSLM) in the reflection mode at a wavelength of 488 nm (Leica TCS SP AOBS). The objective used was a Leica HC PL FLUOTAR 10× with a numerical aperture of NA = 0.3.

2.4.8. Ellipsometry. Spectroscopic ellipsometry data in the visible range was obtained using a UVISEL Jobin Yvon Horiba Spectroscopic Ellipsometer equipped with a DeltaPsi 2 data analysis software. The system acquired a spectrum ranging from 2 to 4.5 eV (corresponding to 300 to 750 nm) with 0.05 eV (or 7.5 nm) intervals. Data were taken using an angle of incidence of 70° and the compensator was set at 45.0°. Data were fitted by regression analysis to a film-on-substrate model as described by their thickness and their complex refractive indices. The values given are averaged over 5 measurements taken on different spots on the surface.

2.5. Local deposition of polypyrrole spots using SECM

The local deposition of polypyrrole using SECM was performed as previously reported.[23,26–29] In short, approach curves for the positioning of the microelectrode to the gold substrate were performed in the monomer solution by poising the tip at $E_T = -0.6$ $V_{Ag/AgCl}$ where the reduction of oxygen is diffusion controlled. The substrate was left at the open circuit potential (OCP). By recording the tip current while approaching the gold substrate (scan rate of 3 μm s^{-1}), the distance between the two electrodes can be determined precisely. For the polymerization a 100 mM pyrrole solution in $LiClO_4$ (0.1 M in water) was used. A potential $E_{app} = 1.3$ $V_{Ag/AgCl}$ was applied for a polymerization time of $\tau = 20$ ms while the distance of the UME to the substrate was $d = 60$ μm.

2.6. Local deposition of polypyrrole dots using E-SNOM

The electro-optical probe was brought into close contact (about 100–50 nm) to the BDD using a shear force based approach. Electropolymerization of a 20 mM pyrrole solution in $LiClO_4$ (0.1 M in water) was performed at $E_{app} = 1.3$ $V_{Ag/AgCl}$ for $\tau = 30$ ms three times for each spot. Scans of an area of 10 μm^2 were performed with a scan rate of 40 μm s^{-1} with a resolution of 100 × 100 pixels.

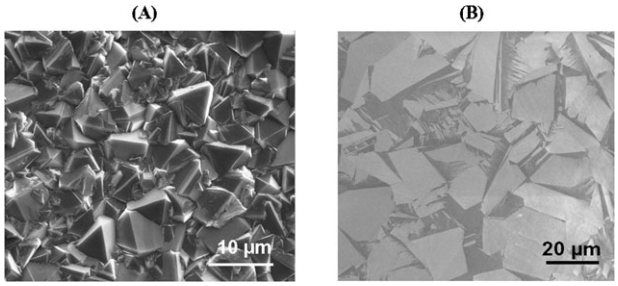

Fig. 1 Scanning electron microscopy images of (A) as-prepared, (B) commercially available polished boron-doped diamond surfaces.

3. Results and discussion

3.1. Surface characterization of silanized BDD interfaces

Fig. 1 shows SEM images of the top view of the samples used in this study. One can see clearly the difference in roughness of the as-deposited polycrystalline diamond film on silicon obtained by PECVD (Fig. 1A) and a commercially available polished freestanding BDD film (Fig. 1B).[22] The contrast in the SEM image of the polished sample arises from the differences in the boron content of the different sectors.[30] The average apparent grain size is between 10 and 50 μm, while structures of different dimensions down to 1 μm in size are also present on the sample. From AFM images a root-mean of about 0.1 nm was calculated. Local electropolymerization was performed on this smooth surface, while the electrochemical characterization and optimization of the polymerization parameters were performed on the rough surface.

The covalent derivatization of BDD with functional silane is depicted in Scheme 1. In the first step the hydrogen-terminated BDD sample was oxidized using UV irradiation for 2 h at room temperature.[10] The photochemical oxidation generates a surface composed of C=O, C–O–C and C–OH groups. The surface hydroxyl groups can be easily coupled to organosilanes under mild conditions. The oxidized BDD surface was reacted with 10^{-3} M hexane/CCl_4 (70/30 v/v) solution of TMPP at room temperature under controlled atmosphere. X-Ray photoelectron spectroscopy (XPS) was used to analyze the chemical composition of the diamond surface before and after chemical modifications and to evaluate the nature of the chemical bonding associated with transformations occurring on the surface. Fig. 2a displays an XPS survey of the hydrogen-terminated BDD surface showing signals due to C 1s at 285 eV and O 1s at 532.6 eV, respectively. The origin of the

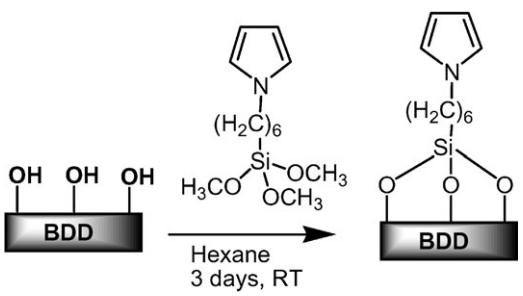

Scheme 1 Chemical functionalization illustration of oxidized BDD with *N*-(3-trimethoxysilylpropyl)pyrrole.

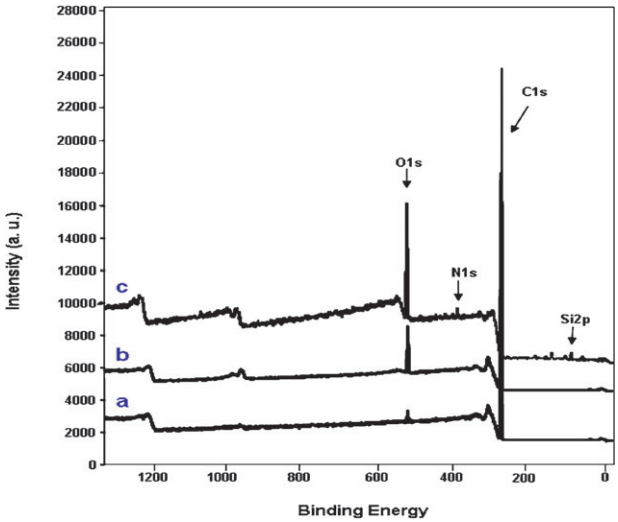

Fig. 2 XPS survey of hydrogenated BDD (a), oxidized BDD (b) and after chemical reaction of oxidized BDD with *N*-(3-trimethoxysilylpropyl)pyrrole (c).

oxygen peak is not clear. It could be assigned to surface contamination or to interstitial incorporation within the C–C back bonds during sample growth (originating from boron oxide used for doping). After UV irradiation in air for 2 h using a low-pressure mercury arc lamp, an increase of the signal of O 1s was observed, consistent with surface oxidation (Fig. 2b). An additional peak due to N 1s and Si 2p (absent in the oxidized BDD surface XPS survey) and a relative increase of O 1s signal were obtained when the oxidized BDD surface was reacted with TMPP (Fig. 2c). The increase of the O 1s signal was not expected since the reaction of the oxidized BDD surface with TMPP should take place without any oxygen incorporation. It is well documented in the literature that parameters such as concentration, solvent quality, temperature, and reaction play an important role in the final morphology and thickness of aminopropylsilane layers onto the surface of oxides.[31,32] The observed high concentration of oxygen in the XPS spectrum (ratio of Si/O = 0.11 instead of 0.33 as expected for a monolayer) is believed to result from multilayers formation. High-resolution XPS spectrum of the oxidized BDD surface displays peaks due to C 1s from the bulk and from the surface C–O features at 285, 287, 288 and 289.2 eV, respectively. Additional peaks at 284 and 286 eV due to C–Si and C–N, respectively, appeared in the high-resolution XPS spectrum after coupling of the surface hydroxyl groups with TMPP molecules. The results are in good agreement with the chemical composition of the layer. The thickness of the TMPP modified BDD was further evaluated using ellipsometry and a mean thickness of 3.95 ± 0.5 nm was obtained. This validates the XPS results and indicates that a multilayer rather than a monolayer (thickness ~1.35 nm) is formed.[33]

3.2. Electrochemical behavior of silanized BDD interfaces

The electrochemical property of the silanized BDD surface was compared to hydrogenated and oxygenated surfaces. Fig. 3 displays cyclic voltammetric *i*–*E* curves for an aqueous

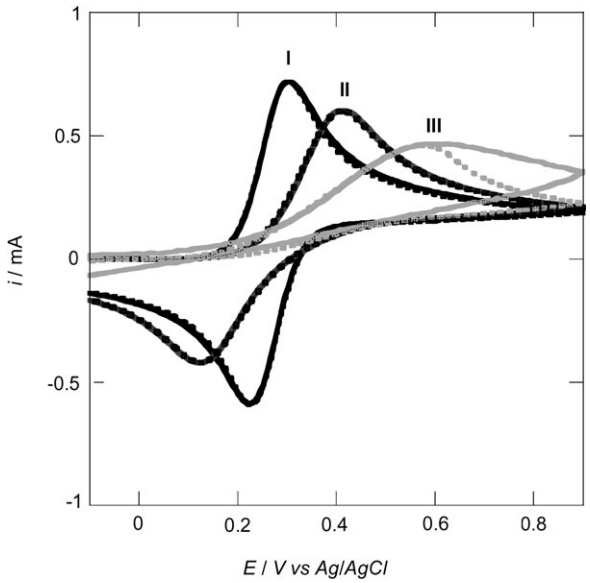

Fig. 3 Experimental (bold lines) and simulated (DigiSim 3.03, dotted lines) cyclic voltammetric *i–E* curves for hydrogenated diamond (I), photochemically oxidized (II), TMPP silanized (III) BDD: solution: $Fe(CN)_6^{4-}$ (10 mM) in KCl (0.1 M)/water, scan rate = 0.1 V s^{-1}, geometric area = 0.315 cm^2.

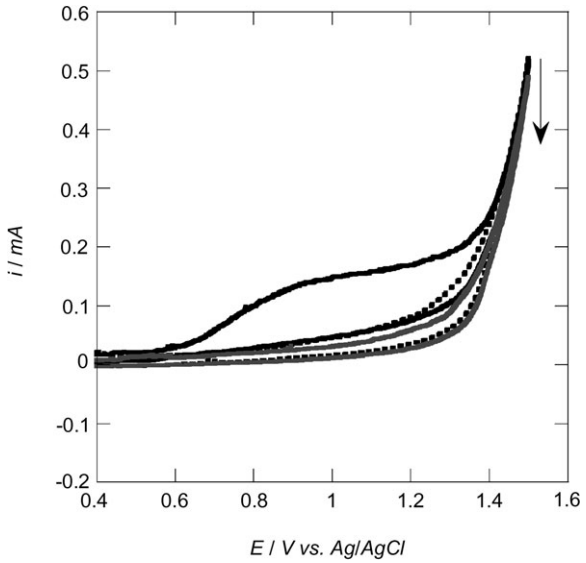

Fig. 4 Subsequent cyclic voltammetric *i–E* curves for TMPP silanized BDD, first scan (black full line), second scan (black dotted line), third scan (grey full line), solution: $LiClO_4$ (0.1 M)/water, A = 0.35 cm^2, scan rate = 0.1 V s^{-1}.

solution of 10 mM $Fe(CN)_6^{4-}$ in 0.1 M KCl at an as-deposited (hydrogenated) BDD electrode before and after photochemical oxidation and silanization. As already reported by us,[10,11] the *i–E* curve for the hydrogenated diamond electrode (Fig. 3, peak I) exhibits a well defined wave with a ΔE_P of 79 mV, while after photochemical oxidation the *i–E* curve not only changes shape but also shows an attenuation of the peak current (Fig. 3, peak II) and an enlarged ΔE_P of 294 mV. This increase in ΔE_P reflects a significant decrease in the apparent rate constant k^0_{app}. The apparent rate constant on the hydrogenated diamond surfaces were determined as k^0_{app} = 0.012 cm s^{-1} while for the oxygenated surface, which is inhibiting the electrode kinetics for $Fe(CN)_6^{4-/3-}$, k^0_{app} = 0.0005 cm s^{-1} was obtained. Through the silanization of the hydroxyl groups with pyrrole units the electrode kinetics for $Fe(CN)_6^{4-/3-}$ is yet more hindered. The obtained $k^0_{app} = 5 \times 10^{-6}$ cm s^{-1} for pyrrole modified BDD differs from that reported by Notus *et al.*[17] for an oxidized BDD electrode modified with aminopropyltriethoxysilane (APTES). The authors reported an enhancement of the $Fe(CN)_6^{4-/3-}$ redox reaction, compared to the observed retardation for the oxidized surface modified with TMPP molecules. This can be explained in terms of a difference in the electrostatic interaction between the surface functional groups (NH_2, pyrrole) and the $Fe(CN)_6^{4-/3-}$ anion. In particular, electrostatic attraction between $Fe(CN)_6^{4-/3-}$ and protonated amino groups at the APTES-treated surfaces are believed to be responsible for the acceleration of the reaction rate.

3.2. Electropolymerization of pyrrole on pyrrolyl-terminated BDD surfaces

The possibility to use pyrrole modified BDD for forming strongly adhesive films of polypyrrole was investigated further. Shown in Fig. 4A is a series of successive voltammetric scans for the pyrrole-modified BDD surface in $LiClO_4$–water electrolytic medium. During the first potential scan, an irreversible broad anodic peak centered at E_p = 1.08 $V_{Ag/AgCl}$ is observed. This compares well with anodic peaks found around E_p = 1 $V_{Ag/AgCl}$ for 1-(2-acetylaminoethyl)pyrrole and *N*-alkylsubstituted pyrroles (generally oxidized at about 200 mV lower).[34] The more difficult oxidation of the pyrrole can be ascribed to resistive effects in the oxygenated BDD surface. These effects are even stronger for the insulating alkyl chains connecting the underlying BDD with the pyrrole heads. In the second scan the anodic peak has already disappeared, indicating that all the electrochemically accessible monomer pyrrole sites in the organic layer have been oxidized. From the electrical charge of the CV of the oxidation step of the polymer matrix and assuming 100% polymerization efficiency, the number of electropolymerizable polymer units can be estimated according to $Q_a = n\delta F$, where F is the Faraday constant, and δ the positive charge per pyrrole unit. Assuming that δ in the range of 0.25–0.35 as usually reported for most *N*-substituted polypyrrole films,[35] n is estimated as being 3.97×10^{-11} mol cm^{-2} and thus a surface coverage of 2.39×10^{13} molecules cm^{-2}.

3.3. Fabrication of polypyrrole nanostructures from localized electropolymerization reaction

A. Scanning electrochemical microscope. The local electropolymerization of the silanized polycrystalline BDD electrodes in the presence of pyrrole monomer was achieved using SECM in the direct mode.[23,26] The choice of the pulsing time as well as the potential where the polymerization takes place and the distance between microelectrode and gold surface is crucial for the formation of homogeneous pyrrole deposits. Fig. 5A shows a confocal scanning laser microscopy (CSLM)

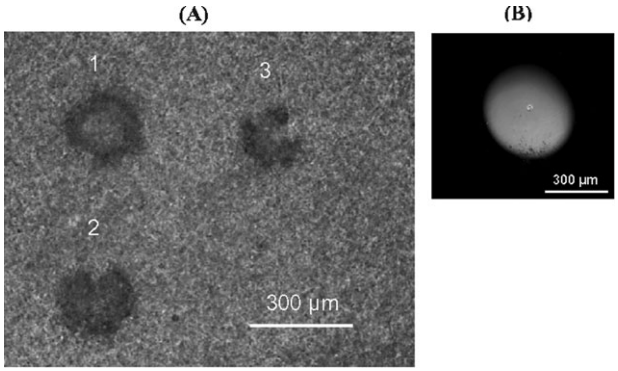

Fig. 5 (A) Confocal scanning laser microscopy reflectance image of an array of pyrrole spots, Spotting conditions: $c_{pyrrole}$ = 100 mM in $LiClO_4$ (0.1 M)/water, z = 60 μm, E_{app} = 1.3 $V_{Ag/AgCl}$, τ = 20 ms; spots 1 and 2 = 3 pulses, spot 3 = 2 pulses; (B) the used UME, diameter of Pt disk = 25 μm, diameter of insulating glass shield = 300 μm.

reflectance image of three polypyrrole spots formed on the pyrrolyl-terminated BDD surface. The diameter of the polymer spots is about 270 μm and is rather independent of the number of potential pulses applied (between two and three pulses of 20 ms) and thus on the amount of electrical charge passed between tip and substrate. The size of the polymer spot corresponds to the diameter of the glass sheath r_{glass} of the UME being 300 μm (Fig. 5B). From the electrical charge,[36] corrected by charging currents, the effective thickness of the polymer film can be estimated as being: 14 nm (spot 3) , 26 nm (spot 2) and to 41 nm (spot 1), respectively.

B. Electrochemical-SNOM. To accomplish E-SNOM (Fig. 6A) incorporating a tuning fork transducer[37,38] the most important feature is the design and construction of a probe tip, which can serve not only as a light source, but also as a nanoelectrode. We followed an approach described in the literature for nanoelectrode formation.[39–42] In short, it includes heating, pulling of the optical fiber, coating with gold and electrical insulation *via* deposition of a cathodic electrophoretic paint consisting of a solution of charged micelles of NH_2 bearing polymer chains suspended in aqueous solution. The paint solution is kept acidic so that the amine groups remain protonated, ensuring the solubility of the micelles. The deposition of the film was triggered by scanning the potential from 0 to −2.5 V at a scan rate of 20 mV s^{-1}. At such cathodic potentials the protons are reduced and the ensuing local rise of the pH triggers the precipitation of the deprotonated chains onto the gold-coated fiber. Thermal curing enables the primary amines to react with diisocyanates present in the paint composition and to crosslink.[43]

The formed opto-electrochemical probe was characterized using cyclic voltammetry (10 mM $Fe(CN)_6^{4-}$ in 0.1 M KCl, v = 10 mV s^{-1}) (Fig. 6B). Assuming that the exposed surface is spherical, the plateau current is related for a single electron process to the sphere r by $i_{lim} = 4\pi FDcr$, with F the Faraday constant, D the diffusion coefficient of $Fe(CN)_6^{4-}$ ($D = 7.6 \times 10^{-6}$ cm^{-2} s^{-1})[44] and c the bulk concentration. Tips with apparent radii between about 10 and 200 nm could be

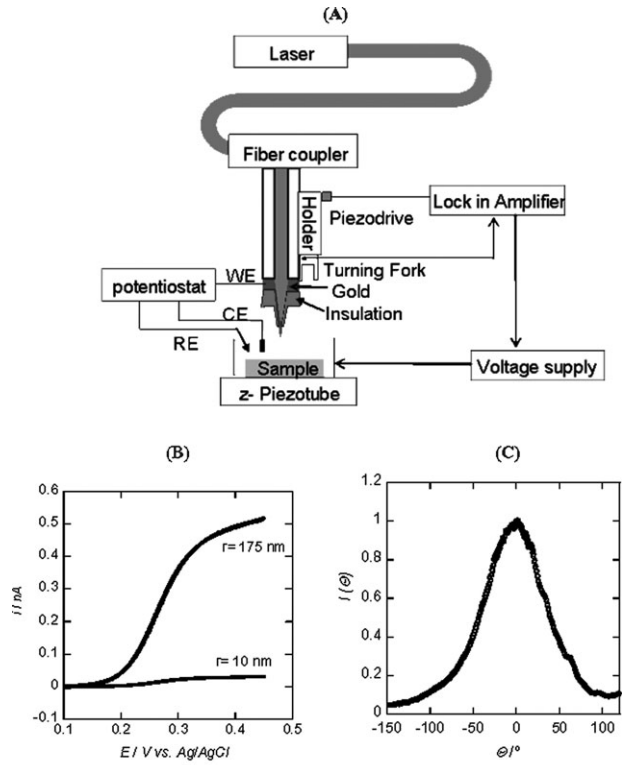

Fig. 6 (A) Schematic, simplified drawing of the electrochemical scanning near-field optical microscope (E-SNOM); (B) cyclic voltammograms of two electro-optical probes fabricated through pulling, gold-coating and insulating an optical fiber with one layer of electrophoretic paint (r = 175 nm) and 3 layers (r = 10 nm), solution: aqueous solution of $Fe(CN)_6^{4-}$ (10 mM) /KCl (0.1 M), scan rate = 10 mVs^{-1}; (C) normalized angular dependency of the transmitted light intensity $I(\Theta)$ for the electro-optical tip.

obtained depending on how many insulating layers were deposited.

Optically the electro-optical probe was characterized by determining the far-field angular intensity distribution $I(\Theta)$ (λ = 633 nm) transmitted through the electro-optical tip (Fig. 6C).[25] The full width at half-maximum (FWHM) of $I(\Theta)$ is characteristic of the aperture diameter (2a) and an aperture size of 380 nm was obtained. The light intensity output through the electro-optical aperture varies from 3 μW (λ = 514 nm, P = 30 mW) to 2 nW (λ = 459 nm, P = 2 mW).

The E-SNOM nanopatterning of BDD modified with TMPP molecules was achieved through local electrochemical deposition in the presence of pyrrole as for SECM studies. The main differences between the SECM and the E-SNOM approaches are: (i) a polished polycrystalline BDD sample was used (Fig. 1B) being adequate for nanometric patterning; (ii) instead of a microelectrode serving as counter electrode, the electro-optical tips were used; (iii) tip–substrate distance was controlled using a shear force approach. Before the patterning step, an E-SNOM image in the pyrrole monomer solution was recorded of the BDD sample surface to ensure that no particles or other impurities adhere to the surface (Fig. 7A). The E-SNOM image confirmed the nanometric roughness of the surface previously reported by us using AFM.[30] After local

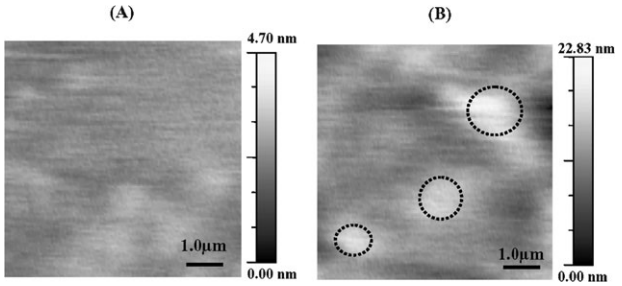

Fig. 7 E-SNOM image of polished and TMPP silanized BDD interface in aqueous solution of pyrrole (A) before spotting, (B) after spotting, scan rate: 40 μm s^{-1}.

electropolymerization, the same area was imaged in solution and revealed some local polymeric structures (Fig. 7B). The diameter of the conducting polymer structure is 1 ± 0.1 μm, thus an order of magnitude smaller than in the case of SECM. As pointed out by Bard *et al.*[45] for SECM in the feedback mode, the size of the sample's surface which interacts most strongly with a microelectrode depends on the distance between the microelectrode and the interacting surface (z) as well as on the dimension of the microelectrode (r): $d_{min} = 2r + 1.5z$. This estimation is as well valid for E-SNOM and represents an estimation to describe the resolution limit (d_{min}) using E-SNOM for deposition studies. For z = 80 nm and an electro-optical tip of 180 nm the minimal spot size which will be obtained with this method is around 480 nm, about half of the size observed. It seems that propagation of polymerization is rather fast leading to larger polymer deposits. However, the shape of the deposits is less well defined as in the case of SECM. This is not too unexpected, as the insulating glass around the microelectrode in SECM confines the polymerization reaction to the volume between tip and sample, while in E-SNOM no such strict thin layer configuration is possible. Nonetheless, while the coupling of SNOM with electrochemistry has already been reported,[46–48] we have to our knowledge shown for the first time that E-SNOM is capable of formation and at the same time imaging micrometric structures in solution.

4. Conclusion

In conclusion, we have shown that the kinetic on boron-doped diamond is highly dependent on the nature of the BDD surface termination. Pyrrole-silanes proved to be important for the formation of strongly adherent polymer films on the BDD surface. Local patterning of the silanized BDD surface was possible using SECM as well as E-SNOM. Indeed, E-SNOM has been used for the first time for the local deposition of a conducting polymer patterns on the micrometer scale as well as for imaging of the polymer pattern in solution. The combination of an electrochemical method with an optical one is of particular interest for studying photochemically induced redox reactions and electrochemically initiated photoactivation and for imaging of complex processes on the surface. E-SNOM would allow (i) electrochemical addressing of specific redox molecules; (ii) photochemical addressing of specific species; (iii) fluorescence detection; and (iv) electrical detection. Moreover, such a multi-probe approach will enable to combine all four processes providing a highly versatile imaging technique with nanometer spatial resolution. Conducting polymers could be further linked to biological molecules such as oligonucleotides. This contribution could open the way to nm-sized DNA arrays with an increased probe density. The fabrication of such an array together with the hybridization detection in the near field is under investigation.

Acknowledgements

The Agence Nationale de la Recherche (''BIODIAM'' project) is gratefully acknowledged for financial support. We would like to thank B. Marcus and M. Mermoux for providing us with two polycrystalline diamond samples as well as S. Huant and R. Herino for making their experience in SNOM accessible for our studies. The authors thank L. Gengembre for the XPS measurements. SS thanks the Hanse Wissenschaftskollege for a 3.5 months fellowship.

References

1 M. C. Granger, M. Witek, J. S. Xu, J. Wang, M. Hupert, A. Hanks, M. D. Koppang, J. E. Butler, G. Lucazeau, M. Mermoux, J. W. Strojek and G. M. Swain, *Anal. Chem.*, 2000, **72**, 3793.
2 D. A. Tryk, K. Tsunozaki, T. N. Rao and A. Fujishima, *Diamond Relat. Mater.*, 2001, **10**, 1804.
3 R. G. Compton, J. S. Foord and F. Marken, *Electroanalysis*, 2003, **15**, 1349.
4 I. Troster, M. Fryda, d. Hermann, L. Schafer, W. Hanni, A. Perret, M. Blaschke, A. Kraft and M. Stadelmann, *Diamond Relat. Mater.*, 2002, **11**, 640.
5 J. A. Carlisle, *Nat. Mater.*, 2004, **3**, 668.
6 T. L. Lasseter, B. H. Clare, N. L. Abbott and R. J. Hamers, *J. Am. Chem. Soc.*, 2004, **126**, 10220.
7 W. Yang, J. E. Butler, J. N. Russell and R. J. Hamers, *Langmuir*, 2004, **20**, 6778.
8 G.-J. Zhang, K.-S. Song, Y. Nakamura, T. Ueno, T. Funatsu, I. Ohdomari and H. Kawarada, *Langmuir*, 2006, **22**, 3728.
9 E. Fortin, J. Chane-Tune, P. Mailley, S. Szunerits, B. Marcus, J.-P. Petit, M. Mermoux and E. Vieil, *Bioelectrochemistry*, 2004, **63**, 303.
10 R. Boukherroub, X. Wallart, S. Szunerits, B. Marcus, P. Bouvier and M. Mermoux, *Electrochem. Commun.*, 2005, **7**, 937.
11 S. Szunerits, C. Jama, Y. Coffinier, B. Marcus, D. Delabouglise and R. Boukherroub, *Electrochem. Commun.*, 2006, **8**, 1185.
12 K. Honda, T. Noda, M. Yoshimura, K. Nakagawa and A. Fujishima, *J. Phys. Chem. B*, 2004, **108**, 16117.
13 K. B. Holt and A. J. Bard, *J. Phys. Chem. B*, 2004, **108**, 15117.
14 A. E. Fischer, Y. Show and G. M. Swain, *Anal. Chem.*, 2004, **76**, 2553.
15 T. Anado, A. Tanaka, M. Ishihara, M. Kamo, Y. Sato, N. Ohashi and S. Shimosaki, *J. Chem. Soc., Faraday Trans.*, 1993, **89**, 3105.
16 D. Delabouglise, B. Marcus, M. Mermoux, P. Bouvier, J. Chane-Tune, J.-P. Petit, P. Mailley and T. Livache, *Chem. Commun.*, 2003, 2698.
17 H. Notsu, T. Fukazawa, T. Tatsuma, D. A. Tryk and Y. Fujiwara, *Electrochem. Solid-State Lett.*, 2001, **4**, H1.
18 H. Notsu, I. Yagi, T. Tatsuma, D. A. Tryk and A. Fujishima, *Electrochem. Solid-State Lett.*, 1999, **2**, 522.
19 P. E. Pehrsson and T. W. Mercer, *Surf. Sci.*, 2000, **460**, 49.
20 R. Boukherroub, *Curr. Opin. Solid State Mater. Sci.*, 2005, **9**, 66.
21 S. Szunerits, Y. Coffinier, S. Janel and R. Boukherroub, *Langmuir*, 2006, ASAP.
22 M. Mermoux, L. Fayette, B. Marcus, N. Rosman, L. Abello and G. Lucazeau, *Diamond Relat. Mater.*, 1995, **4**, 745.

23 C. Kranz, M. Ludwig, H. E. Gaub and W. Schuhmann, *Adv. Mater.*, 1995, **7**, 38.
24 K. Karrai and R. D. Grober, *Appl. Phys. Lett.*, **66**, 1842.
25 C. Obermuller and K. Karrai, *Appl. Phys. Lett.*, 1995, **67**, 3408.
26 C. Kranz, M. Ludwig, H. E. Gaub and W. Schuhmann, *Adv. Mater.*, 1995, **7**, 568.
27 E. Fortin, P. Mailley, L. Lacroix and S. Szunerits, *Analyst*, 2006, **131**, 186.
28 C. Nunes-Kirchner, S. Szunerits and G. Wittstock, *Anal. Chem.*, 2006, submitted.
29 S. Szunerits, N. Knorr, R. Calemczuk and T. Livache, *Langmuir*, 2004, **20**, 9236.
30 S. Szunerits, M. Mermoux, B. Marcus, D. Delabouglise, J.-P. Petit, S. Janel and R. Boukherroub, *J. Phys. Chem. B*, 2006, in print.
31 D. F. Siqueira Petri, G. Wenz, P. Schunk and T. Schimmel, *Langmuir*, 1999, **15**, 4520.
32 K. H. Choi, J. P. Bourgoin, S. Auvray, D. Esteve, G. S. Duesberg, S. Roth and M. Burghard, *Surf. Sci.*, 2000, **462**, 195.
33 K. Seio, W. G. Schmidt, J. Furthmuller and F. Bechstedt, *Phys. Rev. B*, 2002, **66**, 235323.
34 A. F. Diaz, J. Castillo, K. K. Kanazawa, J. A. Logan, M. Salmon and O. Fajardo, *J. Electroanal. Chem.*, 1982, **133**, 233.
35 A. F. Diaz, J. Castillo, K. K. Kanazawa, J. A. Logan, M. Salmon and O. Fajardo, *J. Electroanal. Chem.*, 1982, **133**, 233.
36 B. D. Malhotra, N. Kumar and S. Chandra, *Prog. Polym. Sci.*, 1986, **12**, 179.
37 H. Diesinger, A. Bsiesy, R. Hérino and S. Huant, *J. App. Phys.*, 2001, **89**, 3328.
38 K. E. Schmalenberg, D. M. Thompson, H. M. Buettner, K. E. Uhrich and L. F. Garfias, *Langmuir*, 2002, **18**, 8596.
39 D. W. M. Arrigan, *Analyst*, 2004, **129**, 1157.
40 C. J. Slevin, N. J. Gray, J. Macpherson, V. M. A. Webb and P. R. Unwin, *Electrochem. Commun.*, 1999, **1**, 282.
41 S. Szunerits, J. Tam, L. Thouin, C. Amatore and D. R. Walt, *Anal. Chem.*, 2003, **75**, 4382.
42 S. Szunerits, P. Garrigue, J.-L. Bruneel, L. Servant and N. Sojic, *Electroanalysis*, 2003, **15**, 548.
43 J. Abbou, C. Demaille, M. Druet and J. Moiroux, *Anal. Chem.*, 2002, **74**, 6355.
44 C. Amatore, S. Szunerits, L. Thouin and J. S. Warkocz, *Electrochem. Commun.*, 2000, **2**, 353.
45 A. J. Bard, M. V. Mirkin, P. R. Unwin and D. O. Wipf, *J. Phys. Chem.*, 1992, **96**, 1861.
46 T. Onuki, Y. Watanabe, K. Nishio, T. Tsuchiya, T. Tani and T. Tokizaki, *Jpn. J. Appl. Phys.*, 2002, **41**, 6256.
47 T. Onuki, T. Tokizaki, Y. Watanabe, T. Tsuchiya and T. Tani, *App. Phys. Lett.*, 2002, **80**, 4629.
48 Y. Zu, Z. Ding, J. Zhou, Y. Lee and A. J. Bard, *Anal. Chem.*, 2001, **73**, 2153.